Full-Space Spin-Controlled Four-Channel Metalens With Equal Power Distribution and Broad Bandwidth

*Xiaoluo He, Bowen Ren, Ka Fai Chan, and Alex M. H. Wong**

A novel method is proposed to achieve a multifunctional full-space metalens supporting high power efficiency, broadband operation and large design flexibility for four spin-controlled output channels. A full-space meta-atom comprising an ultra-thin printed circuit board layer and a low-cost 3D-printed dielectric block are introduced. This meta-atom combines the geometric and propagation phase phenomena to divide an incident circularly-polarized wave into four equi-powered output channels (left- and right-polarized reflected waves and left- and right-polarized transmitted waves). The output waveforms can be stipulated with large flexibility by tuning the meta-atoms. The usage of non-resonant phase-tuning mechanisms allows the resultant metalenses to be broadband and power efficient. Two full-space metalenses are demonstrated using this unit cell, where the four output channels carry different combinations of orbital angular momenta and focal lengths. Simulation and experimental results show that, over a broad bandwidth of 50–70 GHz (33%), all channels realize the pre-designed functionalities with high mode purities and achieve an average power efficiency of 90%. Compared to previous multifunctional metalenses, these metalenses offer the simultaneous achievement of full-space operation, spin-decoupled manipulation, high-efficiency and a broad working bandwidth, opening new opportunities for millimeter-wave imaging and communication systems.

1. Introduction

Metalenses, which are a specialized type of metasurface, have demonstrated the ability to flexibly control the amplitude, phase and polarization of incident light beams.[1,2] In recent years, numerous intriguing metalenses have been proposed to achieve aberration correction, diffraction-limited focusing and orbital angular momentum (OAM) generation.[3–7] To enhance the functionality of wavefront control and facilitate compact design, multifunctional metalenses have been developed to enable functional multiplexing.[8–11] One simple approach is to physically merge two or more unit cells with their specified functions. However, this approach has limited efficiency and strong cross-talks between different channels.[12] Another method involves summing the complex amplitude coefficients of the corresponding unit cells for each function, as the far-field distribution of each function can be considered as the Fourier transform of these complex coefficients.[13] More recently, anisotropic structures have been utilized to realize spin-controlled multifunctional metalenses.[14–16] By varying the geometric dimensions and rotation angles of the unit cell, the phase response for orthogonal circularly-polarized (CP) incidences can be decoupled, which simplifies the design process and improves the operational efficiency of multifunctional metalenses.

In the early stages, multifunctional metalenses are limited to operating either in the transmission mode or reflection mode, resulting in the underutilization of half of the electromagnetic space. However, achieving full-space wavefront manipulation is crucial for various applications such as high-capacity communication, forward and backward radar detection and intelligent communication systems. Therefore, numerous types of full-space metalenses have been reported, and these designs can be roughly divided into three categories.[17–28] The first category utilizes the shared-aperture method by merging the reflection and transmission unit cells together, which operates under a single incidence and features a simple design but generally exhibits low aperture efficiency.[21–23] The second method employs polarization-multiplexed techniques, enabling metalenses to transmit x- or y-polarized waves while reflecting the orthogonal polarized waves.[17,18] However, this approach requires multilayer structures and often has narrow bandwidth due to the use of resonant phase. The third approach can be classified as the

X. He, B. Ren, A. M. H. Wong
Department of Electrical Engineering
City University of Hong Kong
Hong Kong, SAR, China
E-mail: alex.mh.wong@cityu.edu.hk

K. F. Chan, A. M. H. Wong
State Key Laboratory of Terahertz and Millimeter Waves
City University of Hong Kong
Hong Kong, SAR, China

The ORCID identification number(s) for the author(s) of this article can be found under https://doi.org/10.1002/lpor.202401843

DOI: 10.1002/lpor.202401843

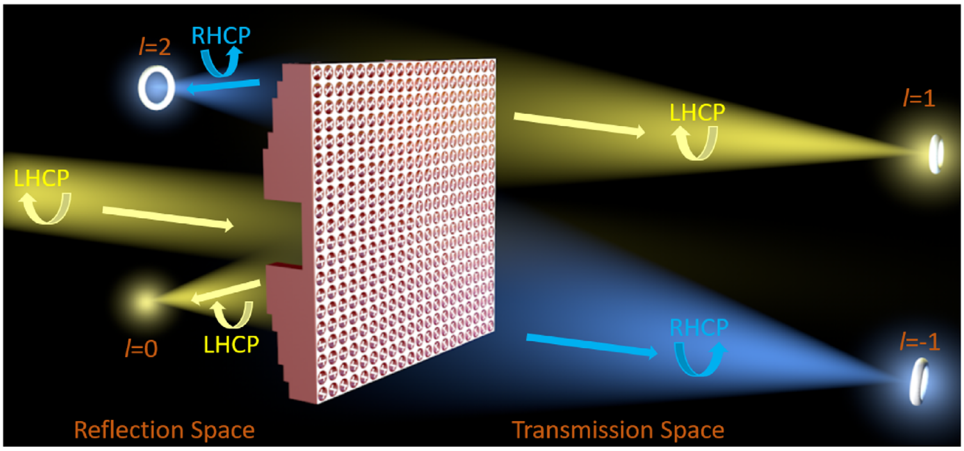

Figure 1. The schematic diagrams of full-space metalens.

frequency-multiplexed method, where full-space manipulation is achieved by carefully tuning the transmission or reflection coefficients at different frequency bands.[19,20] However, these devices also need multiple incidences and suffer from cross-talks between two frequency bands and narrow working bandwidth. Furthermore, some designs combine frequency and polarization-multiplexed techniques to achieve full-space wavefront manipulation, but these structures tend to be more complex and require multiple incidences.[24,25] Among these full-space metalenses, a broadband single-layer metalens has been proposed to realize full-space wave manipulation with only one circularly-polarized (CP) incidence.[27,28] The transmitted cross-polarized wave and reflected co-polarized wave can be manipulated with the geometric phase, but the two channels have spin-locked functions. The other two channels (the transmitted co-polarized wave and reflected cross-polarized wave) cannot be manipulated, resulting in the wastage of half of the incidence power. There is hence a strong demand for a full-space metalens with multifunctionality, a broad working bandwidth and efficient power utilization.

In this paper, we propose a full-space metalens design that enables four channel wavefront manipulation using only a single circularly-polarized (CP) incidence. Our metalens unit cell allows a spin-controlled multifunctionality, equal power distribution of four channels (nearly 25% of each channel) and a broad working bandwidth (50–70 GHz, 33% bandwidth). The unit cell consists of an ultra-thin printed circuit board (PCB) layer and a low cost 3-D printed dielectric block, which can introduce geometric and propagation phases, respectively. Our proposed unit cell offers several advantages compared to previous full-space unit cells.[17–22,24,25,27,28] First, both the single PCB layer and the 3-D printed dielectric block have broad working bandwidths, enabling the combined unit cell to operate across a broad bandwidth (50–70 GHz, 33% bandwidth). Second, for each half-space, the two modulated channels can have spin-decoupled functions: one channel is manipulated solely by the propagation phase while the other channel is tuned by both the geometric and propagation phases. Third, while the transmission and reflection channels have fixed phase response relationships, the four channels can be designed to carry different OAM beams by using the OAM order summation method.[29] Lastly, the unit cell achieves high power utilization, ensuring that the four channels have almost equal power distributions with one incidence, which is advantageous for multi-channel communications. We design two metalenses based on the four channel full-space unit cell. The first metalens achieves beam focusing for both the transmission and reflection half-spaces, but with different focal lengths. Additionally, the two focusing beams in each half-space are spin-decoupled to carry different orbital angular momentum (OAM) orders. The second metalens is designed to generate OAM beams with different orders for the four channels with only one CP incidence ($l = -1, 0, 1, 2$ for LHCP incidence, $l = 1, 2, 3, 4$ for RHCP incidence), as shown in **Figure 1**. Finally, we fabricate and measure both full-space metalenses, and the experimental results align with the numerical and simulation results, demonstrating that our full-space metalenses can achieve spin-controlled multifunctionality with four channels in the full-space and over a broad bandwidth. The design strategy proposed in this research offers great flexibility for designing multifunctional full-space metalenses and opens new possibilities in multi-channel mm-wave communication systems.

2. Full-Space Metalenses Design

In this section, we first introduce the theoretical design of the full-space unit cell, which is capable of separating the CP incidence into four equi-powered channels in the full-space (two reflected waves and two transmitted waves). We then proceed to realize two full-space metalenses with different functions. The first metalens is designed to have different focal lengths for the two half-spaces, while two channels in each half-space are designed to carry different OAM orders. The second metalens is designed with completely different OAM orders ($l = -1, 0, 1, 2$) for the four channels, which enables the generation of multiple OAM modes in both the transmission and reflection spaces. Finally, we present the simulated results of the two full-space metalenses, demonstrating their performance in achieving the desired functions.

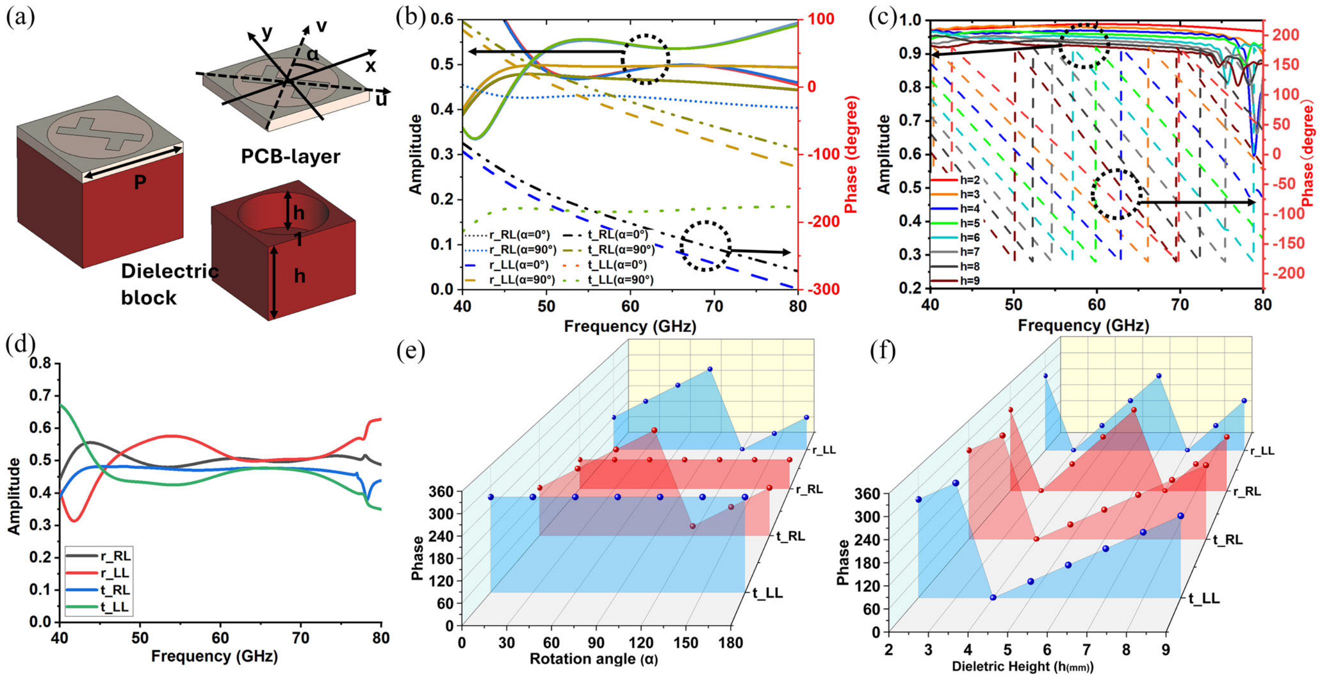

Figure 2. Schematic diagrams of the unit cell. a) The structure of unit cell with a PCB layer and a dielectric block. b) The transmission and reflection coefficients of the solely PCB layer. c) The transmission coefficients of the solely dielectric block. d) The transmission and reflection amplitudes of the complete unit cell. e) Phase changes of four channels respect to the rotation angle (α) at 60 GHz. f) Phase changes of four channels respect to the dielectric height (h) at 60 GHz.

2.1. Theoretical Concept and Unit Cell Design

To achieve comprehensive manipulation of full-space waves under a single CP incidence, we design the unit cell to simultaneously reflect and transmit the incidence to four channels with equal power. Furthermore, we control the output channels of each half-space (transmission space or reflection space) independently to realize the spin-decoupled functions. To address these requirements and ensure a broad working bandwidth, we propose a combined unit cell depicted in **Figure 2a**. It consists of an ultra-thin single printed circuit board (PCB) layer and a 3-D printed dielectric block, which have stable material properties and can be extended to THz (300 GHz), albeit with slightly higher loss, as shown in the Supporting Information. This drawback can be alleviated by choosing a lower-loss dielectric for a THz metalens. In the mm-wave full-space metalens design, the lateral size of the unit cell is $P = 2.5$ mm = 0.5 λ_c, where λ_c is the wavelength at the center frequency of 60 GHz.

We first analyze the transmission and reflection coefficients of the PCB layer using Jones matrices. The PCB layer of the unit cell comprises of a metallic layer and an ultra-thin substrate (Rogers RO5880C) with dielectric constant $\varepsilon_r = 2.2$ and thickness $t = 0.254$ mm. The metallic pattern exhibits n-fold rotational symmetry (n > 2), which allows it to facilitate cross-polarization conversion. Despite its simplicity, the PCB layer can realize four output channels (transmitted co- and cross-polarized waves, reflected co- and cross-polarized waves) with equal power under one circular polarized (CP) incidence. By tuning the rotation angle α, additional geometric phases can be imparted to the transmitted cross-polarized channel and reflected co-polarized channel. These phases are equal to double the rotation angle (α) of the n-fold structure. The phenomenon can be explained using the Jones matrix. Assuming the reflection and transmission coefficients of the unit cell are represented as:

$$R_{uv} = \begin{pmatrix} r_{uu} & r_{uv} \\ r_{vu} & r_{vv} \end{pmatrix} \qquad T_{uv} = \begin{pmatrix} t_{uu} & t_{uv} \\ t_{vu} & t_{vv} \end{pmatrix} \tag{1}$$

where u, v represent the slow and fast axes of the unit cell, r_{ij} (t_{ij}) represent the reflection (transmission) complex coefficients from incident direction j to scattered direction i. R and T is the linear Jones matrix, and it can be easily transformed to the CP Jones matrix ($\widetilde{R}$ and $\widetilde{T}$).

$$\widetilde{R} = M(-\alpha) \cdot R_{uv} \cdot M(\alpha) \qquad \widetilde{T} = M(-\alpha) \cdot T_{uv} \cdot M(\alpha) \tag{2}$$

where

$$M(\alpha) = \begin{pmatrix} \cos(\alpha) & \sin(\alpha) \\ -\sin(\alpha) & \cos(\alpha) \end{pmatrix} \tag{3}$$

is the transfer matrix between the u-v coordinate and the x-y coordinate. Therefore, the transmission field and reflection field under the CP incidence can be expressed as:

$$\begin{pmatrix} E_t^+ \\ E_t^- \end{pmatrix} = \frac{1}{2}\begin{pmatrix} [t_{uu}+t_{vv}+i(t_{uv}-t_{vu})] & [t_{uu}-t_{vv}-i(t_{uv}+t_{vu})]e^{-j2\alpha} \\ [t_{uu}-t_{vv}+i(t_{uv}+t_{vu})]e^{j2\alpha} & [t_{uu}+t_{vv}-i(t_{uv}-t_{vu})] \end{pmatrix}\begin{pmatrix} E_{in}^+ \\ E_{in}^- \end{pmatrix}$$
$$\begin{pmatrix} E_r^+ \\ E_r^- \end{pmatrix} = \frac{1}{2}\begin{pmatrix} [r_{uu}+r_{vv}+i(r_{uv}-r_{vu})] & [r_{uu}-r_{vv}-i(r_{uv}+r_{vu})]e^{-j2\alpha} \\ [r_{uu}-r_{vv}+i(r_{uv}+r_{vu})]e^{j2\alpha} & [r_{uu}+r_{vv}-i(r_{uv}-r_{vu})] \end{pmatrix}\begin{pmatrix} E_{in}^+ \\ E_{in}^- \end{pmatrix} \tag{4}$$

where − and + represents the right-hand-circular-polarized (RHCP) and left-hand-circular-polarized (LHCP), respectively. It can be found that for each incidence, there are four output non-zero channels if the cross-polarization conversation is introduced by the n-fold (n > 2) structure. For the ideal case, the transmission and reflection coefficients are $|t_{uu}| = |t_{vv}| = |t_{uv}| = |t_{vu}| = |r_{uu}| = |r_{vv}| = |r_{uv}| = |r_{vu}| = 0.5$, and $\angle(t_{uu}) = \angle(t_{vv}) = \phi_1, \angle(t_{uv}) = \angle(t_{vu}) = \phi_2, \angle(r_{uu}) = \angle(r_{vv}) = \phi_3, \angle(r_{uv}) = \angle(r_{vu}) = \phi_4$. Assuming the incidence is LHCP (+), the four output channels can be expressed as:

$$\begin{pmatrix} E_t^+ \\ E_t^- \\ E_r^- \\ E_r^+ \end{pmatrix} = \frac{1}{2}\begin{pmatrix} e^{j\phi_1} \\ ie^{j(\phi_2+2\alpha)} \\ e^{j\phi_3} \\ ie^{j(\phi_4+2\alpha)} \end{pmatrix}\left(E_{in}^+\right) \tag{5}$$

From Equation (5), it can be found that four output channels have the same power under the LHCP incidence, while only the transmitted cross-polarized channel (t_{RL}) and reflected co-polarized channel (r_{LL}) possess the additional geometric phase. Figure 2b provides complex coefficients of the four channels with different rotation angles (α) under the LHCP incidence. It can be observed that the amplitudes of the four channels remain constant within the range of [0.45, 0.55] from 50 to 70 GHz, regardless of the rotation angles. Furthermore, as the rotation angle (α) varies, the phases of the transmitted cross-polarized channel (t_{RL}) and reflected co-polarized channel (r_{LL}) exhibit the geometric phase modulations with the same sign. Conversely, the phases of the transmitted co-polarized channel (t_{LL}) and reflected cross-polarized channel (r_{RL}) remain unchanged with the rotation angle (α) changes. The introduced geometric phase allows for the manipulation of two out of the four channels (t_{RL} and r_{LL}), but these two channels are locked to have the same function, leading to the same beam deflection angle or the same OAM beams for transmission and reflection half-spaces.[27,28]

Although the ultra-thin PCB layer is capable of generating four channels under a single CP incidence, two challenges remain. First, for each half-space, only one channel can be modulated with the geometric phase, resulting in half of the incident power being unmodulated. Second, the two modulated channels experience the same modulation and cannot be decoupled solely by the geometric phase. To address these challenges, we introduce a dielectric block that provides propagation phase modulation. This enables the modulation of all four channels and allows for the decoupling of each half-space. The dielectric block, with heights comparable to the wavelength, can be considered as a truncated waveguide.[4] The modulation of the propagation phase is directly dependent on the dielectric constant and height of the block. Furthermore, the dielectric block offers advantages such as robust performance, low fabrication cost and a broad working bandwidth when compared to multi-layer metallic structures.[30] Figure 2a gives the schematic of the dielectric block, which includes two air holes with a height of $h_1 = 0.95$ mm on both the top and bottom to improve the transmission performance.[30] The printed dielectric used has a dielectric constant of $\varepsilon_{r1} = 2.66$ and a loss tangent of 0.02. Figure 2c depicts the transmission performance of the dielectric block with different heights (h). It can be observed that when h varies from 2 to 9 mm, a 360° phase coverage range with high transmission amplitude ($|t| > 0.9$) is achieved across a broad frequency range from 40 to 70 GHz.

Up until this point, we have proposed two structures that serve different purposes in achieving full-space manipulation of four channels. The ultra-thin PCB layer generates four channels with equal power under the CP incidence and introduces geometric phase modulation with different rotation angles (α) for two channels (transmitted cross-polarized and reflected co-polarized). On the other hand, the dielectric block provides the same propagation phase for the two transmission channels (transmitted cross-polarized and transmitted co-polarized) and double that propagation phase for the two reflection channels (reflected cross-polarized and reflected co-polarized). This is because the reflected waves pass through the dielectric block twice, while the transmitted waves only pass through it once. By combining these two structures, all four channels can be manipulated. Figure 2d illustrates amplitudes of four channels under the LHCP incidence, showing stable amplitudes around 0.5 from 50 to 70 GHz, indicating near-equal power distribution among the four channels. We note that, while we design for equal power splitting at the center frequency of 60 GHz, slight variations exist due to the dispersive properties of the PCB layer and a small dielectric loss which changes with the thickness of the dielectric layer. The slight variation in transmission coefficient magnitude is shown, for example, in Figure 2d. Notwithstanding, we shall show in the following that we achieve metalenses with near-equal power splitting (±7%) over the wide bandwidth of 50 to 70 GHz, which compares favorably with existing works,[27,28] and is significant for practical applications. Additionally, only two channels (t_{RL} and r_{LL}) exhibit a geometric phase response, as shown in Figure 2e. Figure 2f displays the phase of the four channels with different dielectric block heights when the LHCP incident to the unit cell from the dielectric side. It can be observed that all four channels demonstrate a propagation phase response, with the phase change of the reflection channels being twice that of the transmission channels when the height of dielectric block changes. Therefore, the final

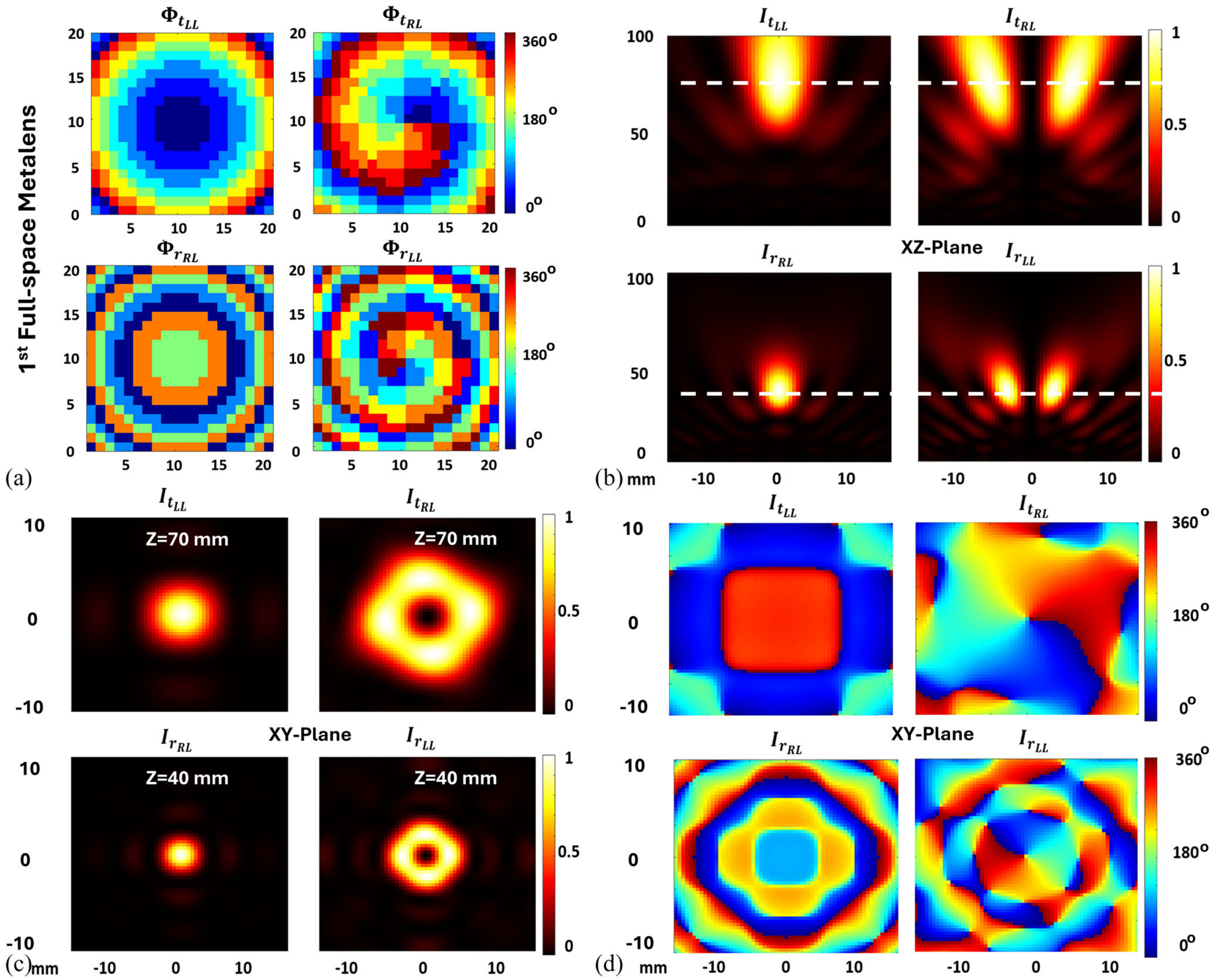

Figure 3. Numerical calculation of the focusing full-space metalens for four channels with a) Phase profiles. b) The intensity distributions along propagation planes. c) The intensity distributions at the focal planes. d) The phase distributions at the focal planes.

four output channels based on the combined unit cell under the LHCP incidence can be summarized as follows:

$$\begin{pmatrix} E_t^+ \\ E_t^- \\ E_r^- \\ E_r^+ \end{pmatrix} = \frac{1}{2} \begin{pmatrix} e^{j(\phi_1+\phi_p)} \\ ie^{j(\phi_2+2\alpha+\phi_p)} \\ e^{j(\phi_3+2\phi_p)} \\ ie^{j(\phi_4+2\alpha+2\phi_p)} \end{pmatrix} \left(E_{in}^+\right) \tag{6}$$

It is important to note that the intrinsic phases (ϕ_1, ϕ_2, ϕ_3, ϕ_4) of the four channels are difficult to manipulate with the ultra-thin single PCB layer.[27,28] However, the combined unit cell utilizes two degrees of freedom to achieve the manipulation of all four channels in the full space: the geometric phase introduced by the PCB layer and the propagation phase introduced by the dielectric post. For each half-space, the two channels (t_{RL} and t_{LL} or r_{RL} and r_{LL}) can be spin-decoupled using the geometric phase. To decouple the channels (t_{RL} and r_{LL} or t_{LL} and r_{RL}) between two half-spaces, the propagation phase is employed, as the phase changes are different. Although the propagation phases of the transmission channels and reflection channels have a fixed relationship, where $r_{\phi_p} = 2\ t_{\phi_p}$, the four channels can now be designed with great flexibility to achieve individual functionalities like focusing to different locations and carrying different OAMs, as we will demonstrate later in the paper.

2.2. Demonstration of Full Space Manipulation

Based on the designed full-space unit cell, we proceed to construct two full-space metalenses. Both metalenses comprises 20×20 unit cells. The first metalens achieves beam focusing in both the transmission and reflection spaces with different focal lengths. In addition, the two channels of each half-space (transmission and reflection) are decoupled to carry different OAM orders. Specifically, under the LHCP incidence, the transmitted LHCP wave focuses with an OAM order $l = 0$ at the focal

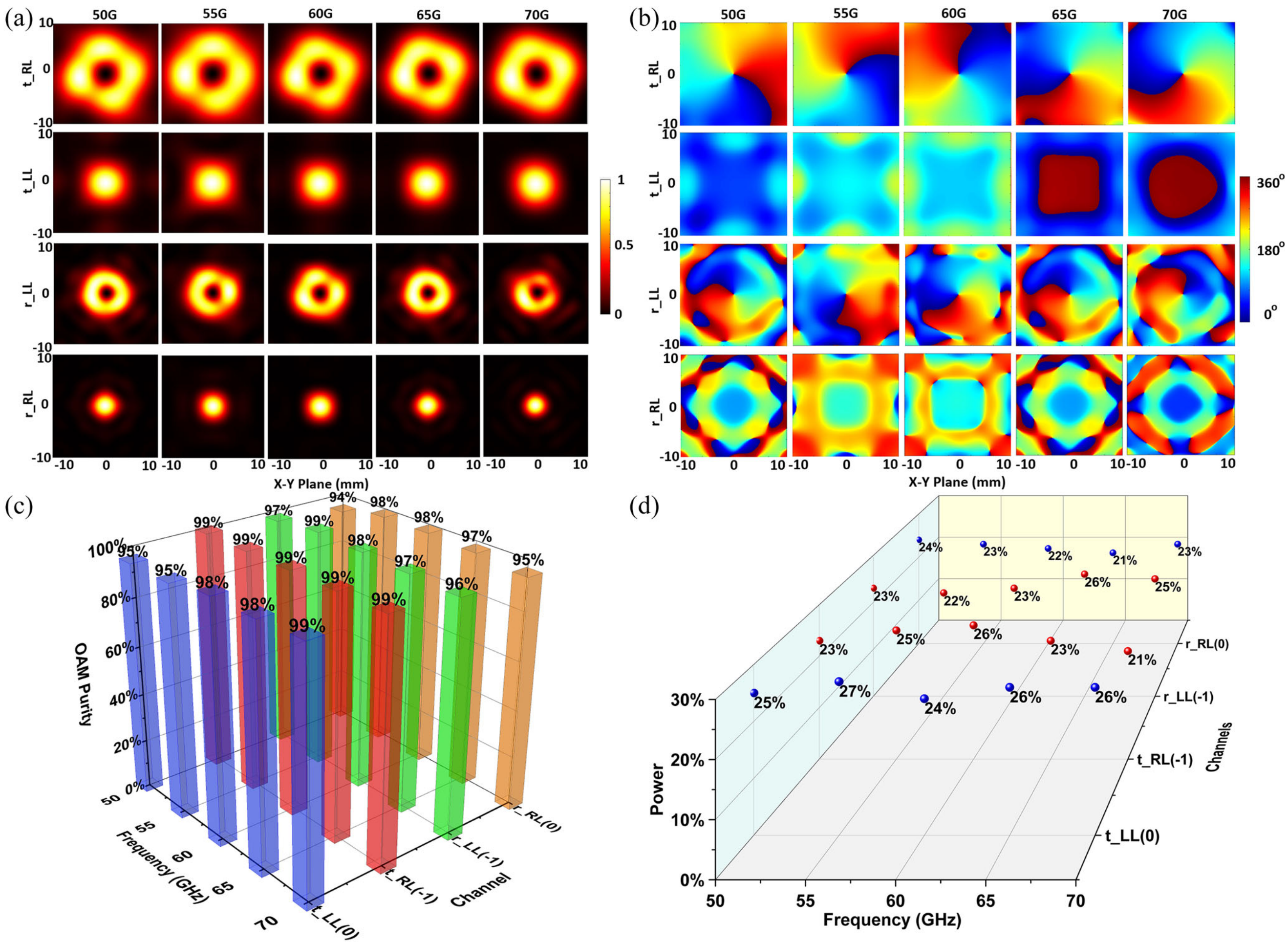

Figure 4. Simulated results for four channels of focusing full-space metalens across the operation bandwidth. a) Intensity distributions. b) Phase distributions. c) OAM purities. d) The transmission and reflection efficiencies.

length of $F_1 = 70$ mm, while the transmitted RHCP wave also focuses at the same focal length F_1 but with a different OAM order $l = -1$. In the reflection space, the reflected RHCP and LHCP channels both focus at the focal length of $F_2 = 40$ mm, with OAM orders of $l = 0$ and $l = -1$, respectively. For the first full-space metalens design, the propagation phase is utilized to provide a hyperbolic phase profile to achieve beam focusing, while the geometric phase is employed to generate the desired OAM orders to decouple the two channels of each half-space. Consequently, the final phase profiles of four channels are as follows:

$$\begin{aligned}
\phi_{t_{LL}} &= -\frac{\omega}{c}\left(\sqrt{F_1^2 + (x^2 + y^2)}\right) - F_1) \\
\phi_{t_{RL}} &= -\frac{\omega}{c}\left(\sqrt{F_1^2 + (x^2 + y^2)} - F_1\right) + l\arctan(y/x) \\
\phi_{r_{LL}} &= -\frac{\omega}{c}\left(\sqrt{F_2^2 + (x^2 + y^2)}\right) - F_2) + l\arctan(y/x) \\
\phi_{r_{RL}} &= -\frac{\omega}{c}\left(\sqrt{F_2^2 + (x^2 + y^2)} - F_2\right)
\end{aligned} \tag{7}$$

where ω is the angular frequency, x and y are the spatial position of the unit cell, F_1 and F_2 represent the focal length of transmission plane and reflection plane, respectively. l is the OAM order of each channel. The phase profiles of four channels based on Equation (7) are presented in **Figure 3a**.

To evaluate the scattering performance of the four channels, we conduct a numerical study based on the point dipole model to investigate the field distribution of each channel in the full-space metalens.[31] Assuming that each unit cell has a uniform amplitude but different phase responses for each output channel, the scattered field by the full-space metalens for different channels can be expressed as:

$$E_{x,y,z} = \sum_{x,y,z} \frac{A}{\sqrt{r}} e^{-j(k_0 r + \phi_{x,y}(i,\omega))} (i = 1, 2, 3, 4) \tag{8}$$

where A is the amplitude and $\phi_{x,y}(i,\omega)$ is the phase of each unit cell for different channels (i = 1, 2, 3, 4) at a specific frequency (ω), r represents the distance from each unit cell to the propagation plane, and k_0 is the wave number. In our first full-space metalens design, under the LHCP incidence, the transmitted and reflected channels can realize beam focusing with focal lengths

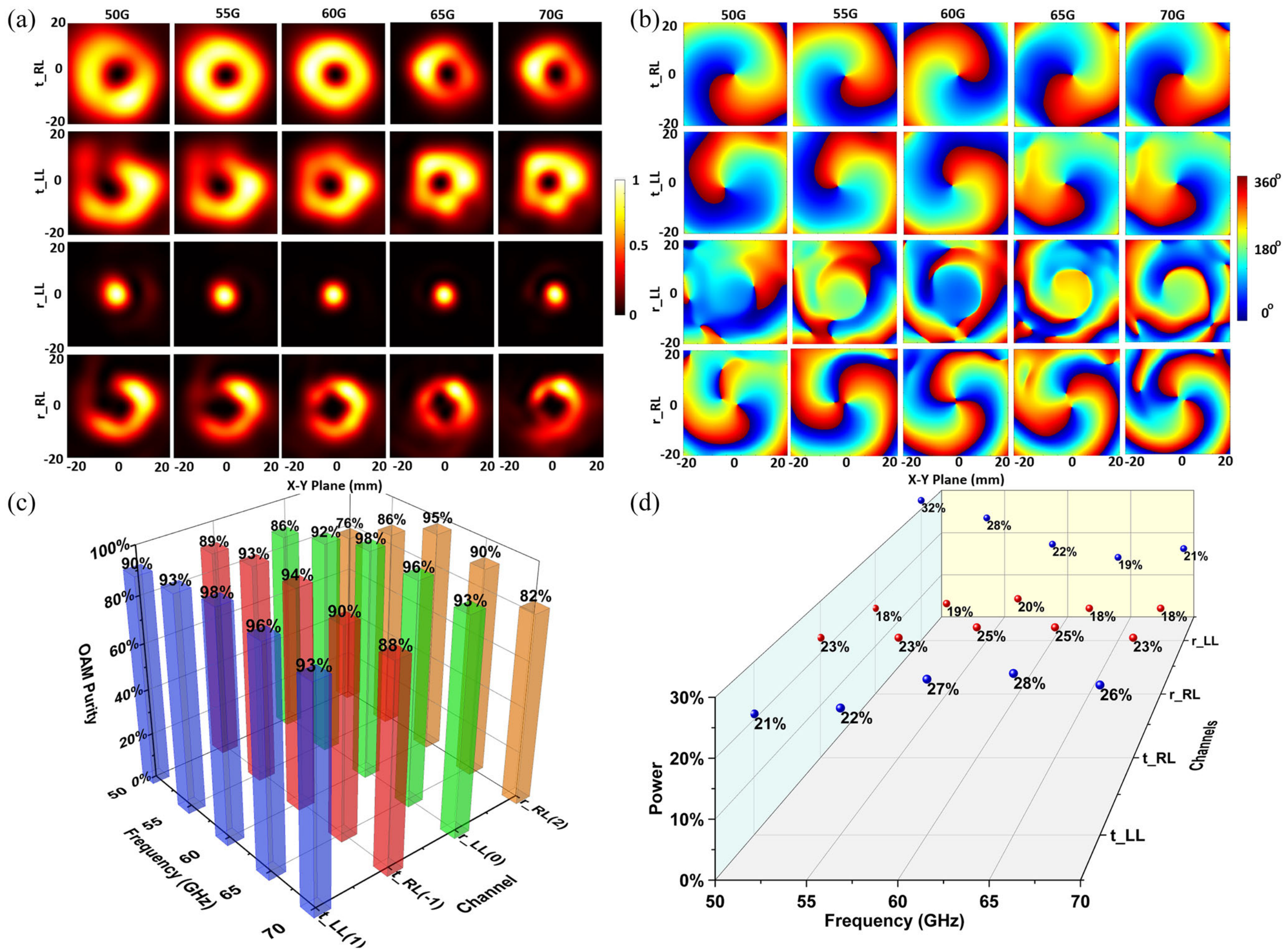

Figure 5. Simulated results for four channels of OAM generation full-space metalens across the operation bandwidth. a) Intensity distributions. b) Phase distributions. c) OAM purities. d) The transmission and reflection efficiencies.

of $F_1 = 70$ mm and $F_2 = 40$ mm, as shown in Figure 3b. While Figure 3c,d shows numerical intensities and phase distributions of four channels at focal planes (x-y plane). It can be observed that two channels of each half-space have focusing beam and vortex beam, respectively. Additionally, the two half-spaces are also decoupled in terms of the focal length.

We carry out full-wave simulations of the two full-space metalenses with the simulation software CST Microwave Studio. A Gaussian beam with LHCP is incident on the metalens from the dielectric side. The x-polarized and y-polarized scattered fields in the full-space are monitored and further used to synthesize different circularly-polarized output channels. The simulated normalized intensity distributions at the focal planes are shown in **Figure 4a**. It can be observed that the two half planes have different sizes of focal spots and OAM beams, as the reflection space of the metalens has a larger numerical aperture ($NA_r = 0.53$) than the transmission space ($NA_t = 0.34$). In addition, two channels in each half-space form a focal spot and a vortex beam, respectively. The focal spots in the transmission space and reflection space at 60 GHz have full-width at half-maximum (FWHM) sizes of 7.8 and 5 mm, which are close to the diffraction limit as determined by $\frac{0.5\ \lambda}{NA}$. Figure 4b gives the phase distributions of four channels across the operation bandwidth, which shows that for each half-space, two channels carry different OAM orders, which are $l = -1$ and $l = 0$, respectively. The OAM purities of different channels across the operating bandwidth are calculated through Fourier transform analysis and shown in Figure 4c (the calculation method is provided in the Supporting Information), indicating high purities of designed beams.[29,32] Figure 4d gives the simulated efficiency of each channel, demonstrating that the full-space metalens effectively separates the incidence into four channels with nearly equal efficiency distribution (which is around 25%). The efficiency is defined as the ratio between the incidence and transmitted/reflected energy of each channel, which can be represented as $\eta_c = \frac{\int E_{ch}^2 ds}{\int E_{inc}^2 ds}$, where the *ch* and *inc* subscripts represent the channel No. and the incidence, respectively.

In the design of the second full-space metalens, we aim to generate four vortex beams with different orbital angular momentum orders for the four channels. First, the propagation phase is designed to have a phase profile corresponding to an OAM or-

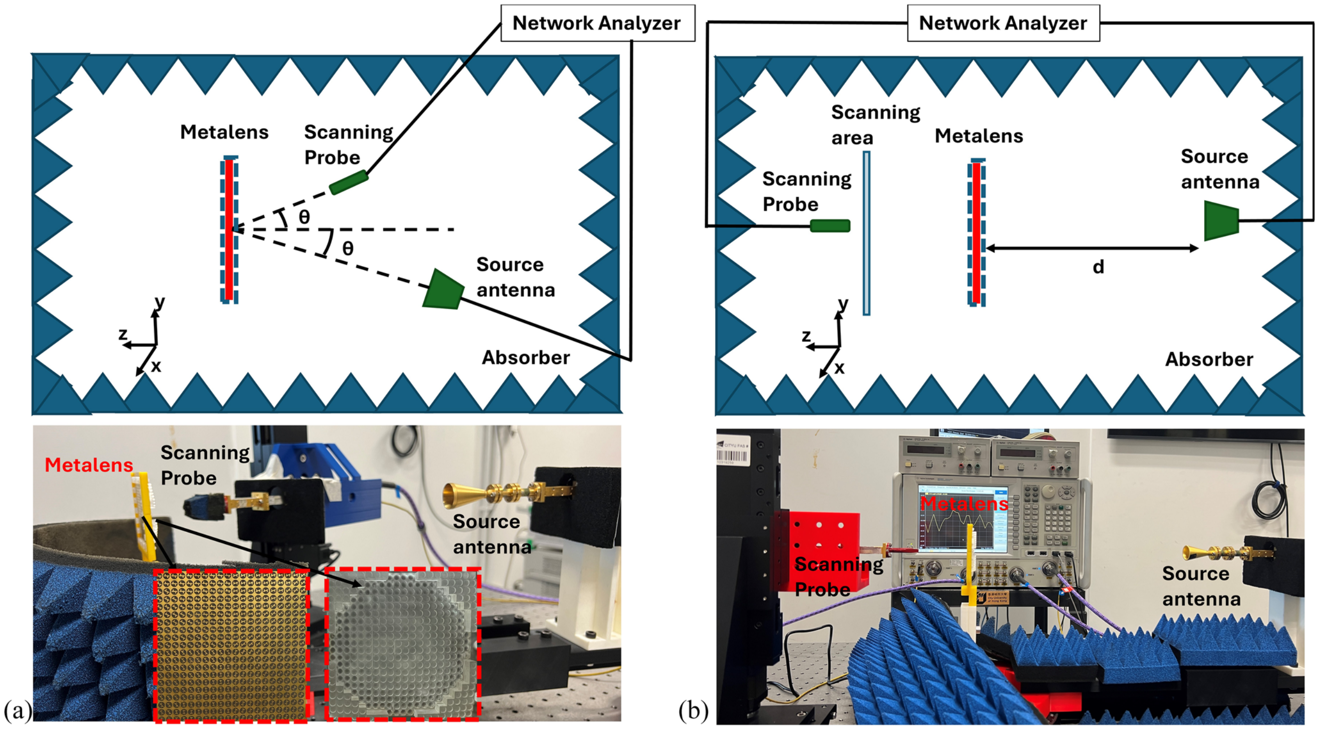

Figure 6. The schematic and photograph of experimental set up for a) the reflection measurement and b) the transmission measurement. (The inset in sub-figure a shows the front and back of the fabricated metalens prototype).

der of $l = 1$. This means that the transmitted LHCP and RHCP channels have the OAM order of $l = 1$, while the reflected LHCP and RHCP channels have the OAM order of $l = 2$ with the modulation of propagation phase. This is because the reflected waves pass through the dielectric block twice, resulting in a doubled OAM order. Next, the geometric phase is introduced with a phase profile corresponding to an OAM order of $l = -2$ for the LHCP incidence. This phase modification is imparted only to the transmitted RHCP channel and the reflected LHCP channel. As a result, the transmitted RHCP channel has an OAM order of $l = -1$, while the reflected LHCP channel has an OAM order of $l = 0$. This decouples the four channels and allows them to have completely different OAM orders ($l = -1, 0, 1, 2$). The numerical calculation process is similar to the first full-space metalens, the process and results can be found in the Supporting Information. The simulated results of the second full-space metalens are given in **Figure 5**. Figure 5a,b shows the intensity and phase distributions of the four channels across the broad bandwidth. From Figure 5b one can infer the different OAM orders carried in the four channels. The OAM purities of the four channels over five frequencies across the operating bandwidth are calculated and shown in Figure 5c. The orders of ($l = -1, 0, 1, 2$) show high purities over the broad bandwidth. The amplitudes of four channels are slightly non-uniform at the edge frequencies (50 and 70 GHz) due to the phase dispersion of the dielectric block. Figure 5d gives the transmission/reflection efficiencies of the four channels, showing nearly equal power distribution among the four channels. In addition, as the geometric phase has opposite signs of phase modulation for orthogonal CP incidences, the geometric phase under the RHCP incidence should have the OAM order of $l = 2$ for the transmitted LHCP channel and the reflected RHCP channel. Therefore, the full-space metalens carries OAM orders of ($l = 1, 2, 3, 4$) under the RHCP incidence, which enlarges the capacities of the generated OAM orders. The details are provided in the Supporting Information.

3. Experimental Section

We proceed to fabricate and characterize the full-space metalenses. **Figure 6** shows the fabricated metalens prototypes and setup for the experiment. The size of the fabricated metalens is 50×50 mm^2. Transmitting circularly-polarized antennas (a 50–58 GHz SGH-15-RC165, a 58–68 GHz SAC-2012-141-S2, and a 68–75 GHz SGH-15-RC125) are placed sufficiently far from the metalens to launch an incident LHCP wave. In the experiment, the metalens is mounted onto a 3D-printed holder and surrounded by absorbers. The central point of the metalens is defined as the origin (x = y = z = 0). Then a linearly-polarized probe is used to scan the electric field distribution along the XYZ-dimensions. For the measurement of each transmission XY-plane or reflection XY-plane, the x- and y-directed electric fields are measured with 1 mm (which is equal to 0.2 λ_c) spatial resolution, and then used to synthesize the transmitted and reflected circularly-polarized fields, while the relatively large step size helps speed up the measurement, we show in the Supporting Information that this step resolution is sufficient for accurately determining the OAM mode purity. Figure 5a shows the schematic for reflection measurement. A small oblique angle ($\theta = 15°$) is added for both the source antenna and the scanning probe to avoid blockage, and the probe is scanned along the -

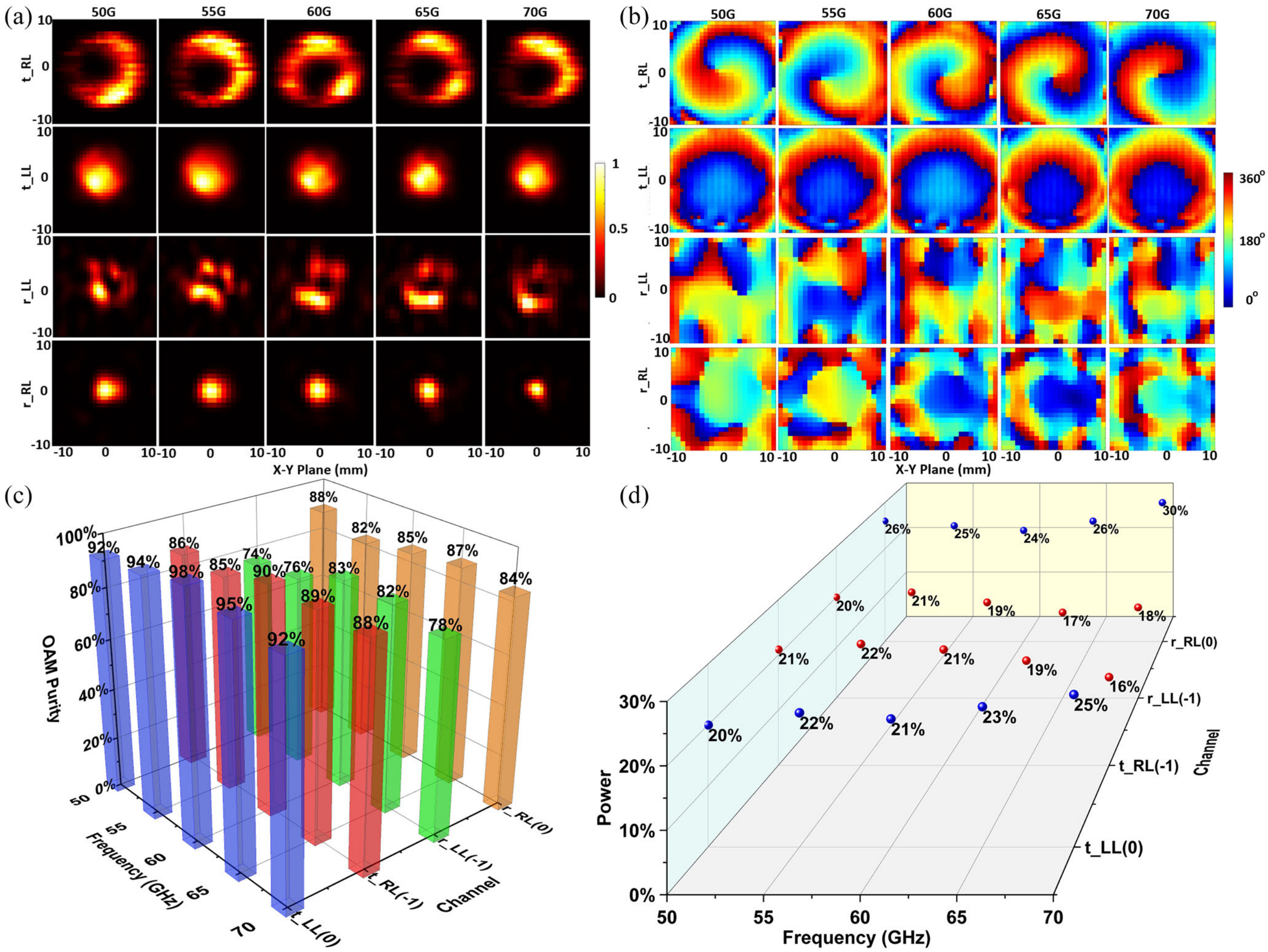

Figure 7. The measured field of focusing full-space metalens: a) Normalized intensity distribution at the focal plane (x-y plane, z = 70 mm). b) Normalized field distribution of the focal plane (x-y plane, z = −40 mm). c) OAM purities of four channels. d) The efficiencies of four channels over the operating bandwidth.

z direction in the reflection measurement. Figure 5b shows the schematic for transmission measurement. The source is placed just at the normal direction of the metalens, and the probe is scanned to collect the transmitted field along the +z direction.

Figure 7 gives the measured results of the first (focusing) full-space metalens under the LHCP incidence. First, we find that the fabricated full-space metalens can generate four channels with different intensity and phase distributions, as shown in Figure 7a,b. The transmission focal plane has a larger focal spot and vortex beam compared to the reflection focal plane. The measured full-width at half-maximum (FWHM) of the focal spots at the center frequency (60 GHz) for transmission and reflection are 8.6 and 5.5 mm, respectively. These values are close to the simulation results. In addition, for each half-plane, the two orthogonal CP channels show clearly different OAM orders, which are consistent with the numerical and simulation results.

Figure 8a,b gives the measured intensity and phase distributions of the observation plane for the second (OAM generation) full-space metalens. The experimental results clearly show that the four channel beams in the full-space have different OAM orders, demonstrating spin-controlled wave manipulation for all four channels in full-space. Compared to the simulation results, the measured OAM beams show slightly elliptical and have non-uniform intensities, especially in the reflected channels. This phenomenon can be summarized into the following three reasons: First, in simulations, we can record the x- and y-polarized components under ideal conditions and synthesize the corresponding circularly polarized (CP) channels. In contrast, in the experiment, we manually rotate the receive linear-polarized probe to measure the x- and y-directed electric fields, which are then used to synthesize the CP fields. This manual process introduces calibration errors. Utilizing a dual-polarized probe and simultaneous multi-port measurement would significantly reduce such errors. Second, simulations assume an ideal Gaussian beam incident on the metalens. However, in the experiment, the field at the metalens plane exhibits about 100° phase dispersions, as shown in Supporting Information, resulting in lower OAM mode purities. Last, the scattered fields of the reflection channels are affected by the oblique incidence, leading to more elliptical intensity distributions compared to the transmis-

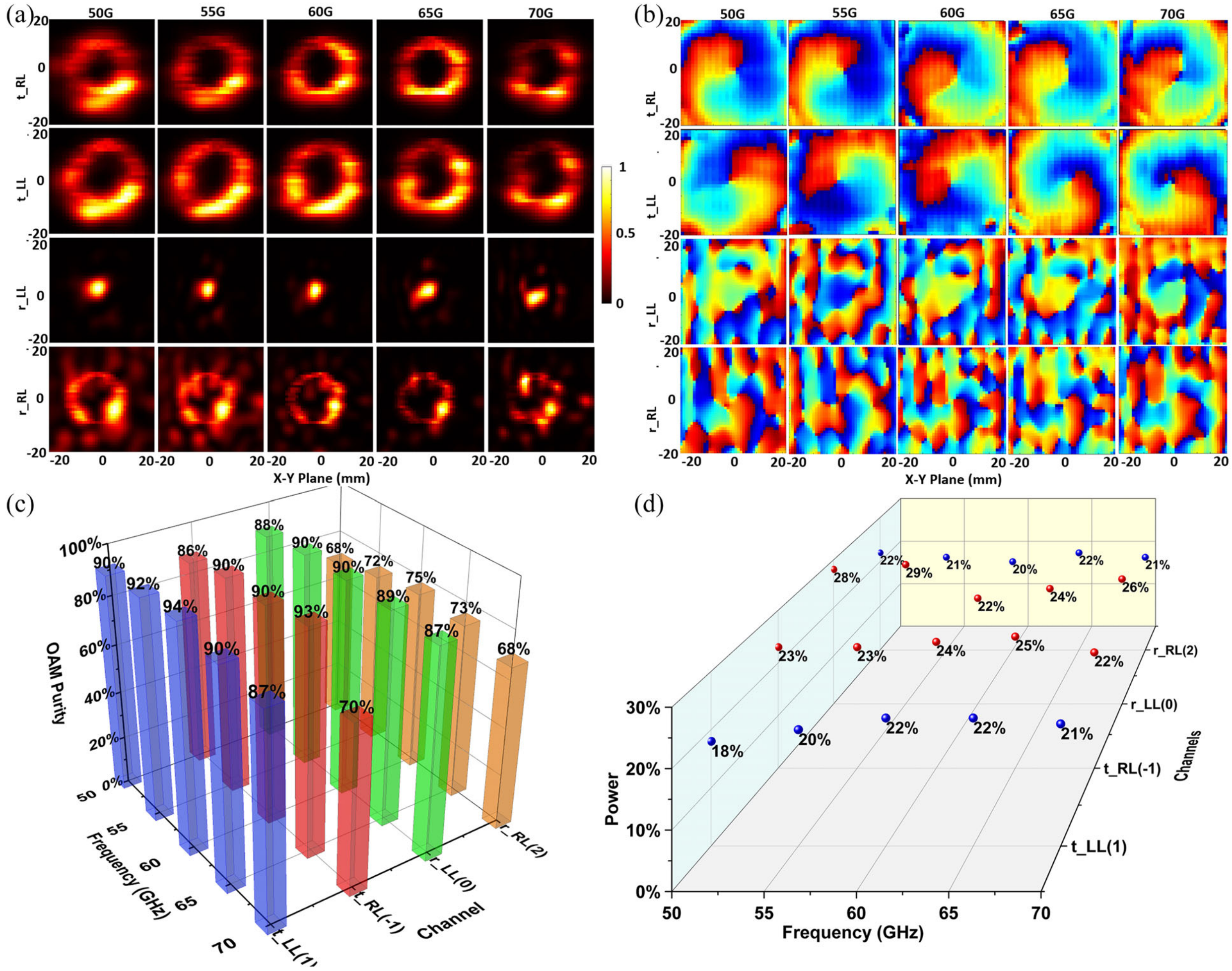

Figure 8. The measured field of OAM generation full-space metalens: a) Normalized intensity distribution at the observation plane (x-y plane, z = 100 mm). b) Normalized field distribution along the focal plane (x-y plane, z = −70 mm). c) OAM purities of four channels. d) The efficiencies of four channels over the operating bandwidth.

sion channels. Figure 7c and Figure 8c plot the OAM purities of the four channels for both full-space metalenses across the operating bandwidth. Although the purities of the experimental results have slightly declined compared to the simulation results, all channels in both cases still maintain high average OAM purities (≥80%) over the broad bandwidth. Figure 7d and Figure 8d show the measured efficiencies of the four channels of each full-space metasurface. Compared to simulation results, we find that the total efficiency of both metasurfaces have slightly reduced, but for both metasurfaces and for all frequencies under test, the power delivered to the four channels combine to around 90% of the incident power, hence demonstrating excellent power efficiency over a large bandwidth. The discussion on efficiency calculation can be found in the Supporting Information. Nevertheless, the efficiency of each channel still maintains a relative equal energy distribution, which is consistent with the unit cell performance.

Table 1 provides a comparison between our full-space metalenses and the most relevant previous works. First, most full-space multifunctional metalenses in the literature require multiple incidences to achieve different functions,[17–19,23–25,27] as they employ polarization-multiplexed or frequency-multiplexed methods. This increases the complexity of the system and may limit the overall performance due to the need to minimize cross-talk between different channels.[17–19,23–25] Furthermore, in these previous works, the efficiency of different functions cannot be controlled, and the overall bandwidth is affected by the performance of each individual function. For example, in Ref. [22], although the transmission mode has a wide bandwidth, the bandwidth of reflection mode is quite narrow due to the resonance phase employed. For another example, Ref. [25] realizes ultra-wideband full-space wave manipulation, but the two manipulated channels have the same function, and the other two channels are unmodulated, resulting in a power efficiency below 50%. In contrast, our design utilizes a simple combined unit cell to achieve spin-controlled OAM beam generation with four channels in the full space. Only one incidence is required, and the power can be equally distributed into the four channels, resulting in high power utilization. Additionally, all four channels of our metalens have the same operation bandwidth, making the overall working

Table 1. Comparison of the proposed metasurface with other representative works.

Ref #	Design Principle	Function-decoupled	No. of incidence	Bandwidth	Efficiency
[17]	Polarization-Multiplexed	Yes	2	10.4–11.2 GHz (7%)	85%
[18]	Polarization-Multiplexed	Yes	3	15 GHz	88%
[19]	Frequency-Multiplexed	Yes	2	8.3 GHz, 12.8 GHz (single frequency)	84%
[23]	Frequency-Multiplexed and Interleaved	Yes	2	11 GHz, 16 GHz	85%
[24]	Polarization and Frequency Multiplexed	Yes	3	16–24 GHz (40%), 37.5–40 GHz (6%)	Not Given
[25]	Polarization and Frequency Multiplexed	Yes	4	8.7 GHz, 15.8 GHz	89%
[27]	Partially Polarization Conversion	No	1	9.3–32.5 GHz (112%)	50%
Our work	Partially Polarization Conversion Combined phase	Yes	1	50–70 GHz (33%)	90%

bandwidth comparable to other full-space metalenses with multiple functionalities.

4. Conclusion

In conclusion, we have proposed a new class of multifunctional full-space metalenses which only require one circularly-polarized incidence. Our design utilizes a combined full-space unit cell comprising an ultra-thin PCB layer and a low cost 3D-printed dielectric block. This unit cell enables the generation of four channels with equal power distribution and spin-decoupled functions in each half-space. By carefully controlling the geometric phase and the propagation phase, we achieve precise wavefront manipulation in the full-space. In contrast to most previous works, our metalenses achieve multifunctionality, broad working bandwidth and spin-controlled modulation with only one incidence. The four channels of our metalenses have equal power distribution and the same operational bandwidth, making our metalenses comparable to other multifunction full-space metalenses. Our proposed metalenses offer simultaneous full-space operation, spin-decoupled manipulation and a broad working bandwidth, which can be applied for various applications in imaging, sensing, and communication systems in the optics to microwave regions.

Supporting Information

Supporting Information is available from the Wiley Online Library or from the author.

Acknowledgements

This work was supported by a Collaborative Research Fund (Grant C6012-20GF) and an Area of Excellence Fund (AoE/E-101/23-N) from the Research Grants Council of Hong Kong.

Conflict of Interest

The authors declare no conflict of interest.

Data Availability Statement

The data that support the findings of this study are available from the corresponding author upon reasonable request.

Keywords

broad bandwidth, full space, metalens, multifunction

Received: October 30, 2024
Revised: January 19, 2025
Published online:

[1] M. Khorasaninejad, F. Capasso, *Science* **2017**, *358*, 8100.
[2] W. X. Tang, J. Chen, T. J. Cui, *Adv. Photon. Res.* **2021**, *2*, 2100001.
[3] S. Wang, P. C. Wu, V. C. Su, Y. C. Lai, M. Chen, H. Y. Kuo, B. H. Chen, Y. H. Chen, T. T. Huang, J. H. Wang, R. M. Lin, C. H. Kuan, T. Li, Z. Wang, S. Zhu, D. P. T. sai, *Nat. Nanotechnol.* **2018**, *13*, 227.
[4] X. Zou, G. Zheng, Q. Yuan, W. Zang, R. Chen, T. Li, L. Li, S. Wang, Z. Wang, S. Zhu, *PhotoniX* **2020**, *1*, 1.
[5] M. K. Chen, Y. Wu, L. Feng, Q. Fan, M. Lu, T. Xu, D. P. Tsai, *Adv. Opt. Mater.* **2021**, *9*, 2001414.
[6] X. He, C. Qi, S. Lei, A. M. H. Wong, *Nanophotonics* **2023**, *12*, 3633.
[7] C. Qi, X. He, B. Ren, A. M. H. Wong, *Adv. Opt. Mater.* **2024**, *12*, 2302459.
[8] S. Chen, W. Liu, Z. Li, H. Cheng, J. Tian, *Adv. Mater.* **2020**, *32*, 1805912.
[9] K. Du, H. Barkaoui, X. Zhang, L. Jin, Q. Song, S. Xiao, *Nanophotonics* **2022**, *11*, 1761.
[10] Y. Li, S. Chen, H. Liang, X. Ren, L. Luo, Y. Ling, S. Liu, Y. Su, S. T. Wu, *PhotoniX* **2022**, *3*.
[11] D. W. Zhang, C. T. Xu, Q. M. Chen, H. Cao, H. G. Yu, Q. G. Tan, Y. Q. Lu, W. Hu, *PhotoniX* **2024**, *5*.
[12] Y. W. Huang, W. T. Chen, W. Y. Tsai, P. C. Wu, C. M. Wang, G. Sun, D. P. Tsai, *Nano Lett.* **2015**, *15*, 3122.
[13] L. Huang, H. Mühlenbernd, X. Li, X. Song, B. Bai, Y. Wang, T. Zentgraf, *Adv. Mater.* **2015**, *27*, 6444.
[14] F. Ding, R. Deshpande, S. I. Bozhevolnyi, *Light Sci. Appl.* **2018**, *7*, 17178.
[15] T. Li, X. Xu, B. Fu, S. Wang, B. Li, Z. Wang, S. Zhu, *Photonics Res.* **2021**, *9*, 1062.
[16] Y. Xu, Q. Li, X. Zhang, M. Wei, Q. Xu, Q. Wang, H. Zhang, W. Zhang, C. Hu, Z. Zhang, C. Zhang, X. Zhang, J. Han, W. Zhang, *ACS Photonics* **2019**, *6*, 2933.
[17] T. Cai, G. Wang, S. Tang, H. Xu, J. Duan, H. Guo, F. Guan, S. Sun, Q. He, L. Zhou, *Phys. Rev. Appl.* **2017**, *8*, 034033.
[18] L. Zhang, R. Y. Wu, G. D. Bai, H. T. Wu, Q. Ma, X. Q. Chen, T. J. Cui, *Adv. Func. Mater.* **2018**, *28*, 1802205.
[19] R. Mao, G. Wang, T. Cai, K. Liu, D. Wang, B. Wu, *Opt. Express* **2018**, *28*, 31216.
[20] L. Bao, X. Fu, R. Y. Wu, Q. Ma, T. J. Cui, *Adv. Mater. Technol.* **2021**, *6*, 2001032.

[21] Y. Wang, Y. Ge, Z. Chen, X. Liu, J. Pu, K. Liu, H. Chen, Y. Hao, *IEEE Trans. Microw. Theory Tech.* **2021**, *70*, 254.
[22] W. Yang, K. Chen, S. Dong, S. Wang, K. Qu, T. Jiang, J. Zhao, Y. Feng, *ACS Appl. Mater. Interfaces* **2023**, *15*, 27380.
[23] S. Wang, G. Zhai, Y. Chen, J. Gao, Y. Zhou, X. Wang, Z. Zhang, J. Ren, *IEEE Trans. Microw. Theory Tech.* **2023**, *71*, 5160.
[24] Y. Pan, F. Lan, Y. Zhang, H. Zeng, L. Wang, T. Song, G. He, Z. Yang, *Photonics Res.* **2022**, *10*, 416.
[25] C. Wang, H. X. Xu, G. Hu, Y. Liu, T. Liu, K. Wang, F. Zhang, X. Shuo, J. Xu, Z. Pang, *Nanophotonics* **2023**, *0*, 416.
[26] C. Yang, G. B. Wu, D. Zheng, K. F. Chan, C. H. Chan, *IEEE Trans. Antennas Propag.* **2023**, *71*, 7804.
[27] M. R. Akram, G. Ding, K. Chen, Y. Feng, W. Zhu, *Adv. Mater.* **2020**, *32*, 1907308.
[28] T. Lu, J. Wu, Z. Shen, Y. Wang, H. Cheng, Y. Li, Y. Yang, H. Yang, *IEEE Trans. Antennas Propag.* **2022**, *70*, 6850.
[29] J. Liu, J. Qi, J. Yao, W. Hu, D. Zhang, H. X. Xu, X. Wang, *Nanophotonics* **2022**, *11*, 2369.
[30] H. Yi, S. W. Qu, K. B. Ng, C. H. Chan, X. Bai, *IEEE Trans. Antennas Propag.* **2015**, *64*, 442.
[31] A. A. Fathnan, T. M. Hossain., D. Mahmudin, Y. N. Wijayanto, D. A. Powell, *IEEE Trans. Antennas Propag.* **2021**, *70*, 2023.
[32] K. Zhang, Y. Yuan, X. Ding, H. Li, B. Ratni, Q. Wu, J. Liu, S. N. Burokur, J. Tan, *Laser Photonics Rev.* **2021**, *15*, 2000351.